

Chapter 12

The Finite Element Method for Porous Materials

12.1. Introduction

12.1.1. *Position of the problem*

To reduce the noise and vibration perturbations, it is beneficial to use the dissipative properties of poroelastic materials. These materials are generally not used alone, but rather inserted in composite mechanical assemblies made of elastic structures, poroelastic materials and air insertions. If these structures are assemblies of layers of materials, they are called multilayer complexes. If the porous material is modified by an addition of solid or fluid inclusions, the term heterogenous porous material is widely used. To predict the vibratory response of such assemblies, closed form solutions can not generally be obtained and the calculation of the vibroacoustic response must then be calculated using numerical techniques.

12.1.2. *Outline of the finite element method*

The finite element method (FEM) is nowadays the most common numerical method used in static and dynamic structures for the resolution of boundary problems. The boundary problem is continuous and the general principle of these numerical methods is to approach this continuous problem with a finite number of degrees of freedom. This method derives its popularity from its flexibility, considering its

general nature or its implementation. Moreover, it is based on convergence theorems from functional analysis, obtaining the validity criteria of the method. However, these mathematical results may be directly interpreted from the physical point of view either as the solution of a minimizing energy problem (provided, however, that some symmetry properties are verified – which is not always the case) or as an analogy with the classical principle of the virtual powers.

Unlike other methods, such as the finite difference method, the discretization is not directly conducted on the partial differential equations themselves, but on an equivalent integral formulation called the variational formulation. The first step of the method is to obtain this variational formulation. The Ω domain occupied by the structure is then divided into a finite number of subdomains called mesh. On each mesh, a number of points called nodes are selected, and a set of functions called interpolation functions are used to calculate the unknown parameters at each element of the mesh according to the values of these parameters at the nodes. The discretized problem is then obtained by writing the relations between the unknown nodal parameters to obtain a linear system of equations. Once this system is solved, it is then possible to determine, represent or use the approached solution. The FEM is described in detail in many books [RAV 98, ZIE 89]. We will focus here on its application to porous materials.

12.1.3. History of the finite element method for porous materials

The FEM began to be used to predict the response of structures involving porous materials in the 1990s. The first formulations proposed involved variables corresponding to the displacements of the solid phase and fluid phase: we can mention the work of Kang and Bolton [KAN 95, KAN 96, KAN 97, KAN 99] or the work of Panneton and Atalla [PAN 96a, PAN 96b, PAN 97]. Other formulations where the displacement of the fluid phase was replaced by a relative displacement between the two phases have since appeared [COY 94, COY 95, JOH 95, VIG 97]. Nevertheless, these formulations based on the movement had the disadvantage of being relatively difficult to implement. It also became apparent that the most intuitive variable to describe a fluid environment was not its displacement, but the pressure. Atalla *et al.* [ATA 98] proposed a mixed formulation displacement-pressure, based on an assumption of harmonic movement, and obtained the first mixed finite element systems for porous materials. Several variations were then derived from the original formulation, each of which is best suited to manage the given boundary or coupling conditions. An exhaustive review was made by Sgard [SGA 02]. The methods based on this formulation are today the most widely used. Nevertheless, although the number of degrees of freedom per node is currently 4 and not 6, the systems obtained by this method are still large, and, of course, frequency-dependent. More recently, works in functional analysis have been conducted to justify the existence of such solutions, but also to deal in an optimal manner, the stages of discretization and thereby to reduce the numerical cost of the method [HÖR 03].

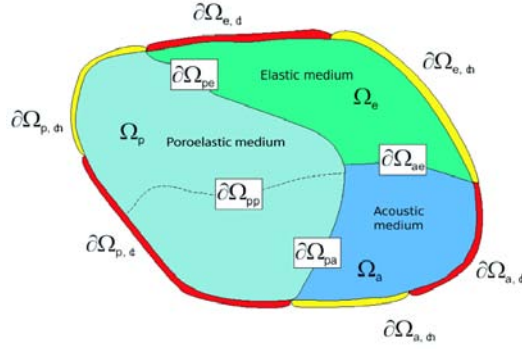


Figure 12.1. Coupled problem

12.1.4. Continuous problems considered

Biot’s theory provides us with a set of partial differential equations and boundary conditions governing the homogenized porous material. Figure 12.1 presents a coupled, poro-elasto-acoustic, three-dimensional problem. It is here a composite structure made of structures of various kinds; porous material, elastic solid and acoustic cavities. Each subdomain is described by a set of partial differential equations and boundary conditions at the borders that reflect the continuity relationships.

We will describe them using the formulations $\{\mathbf{u}, \mathbf{U}\}$ and $\{\mathbf{u}, P\}$.

We will consider a poroelastic sub-structure occupying an area (Ω) of the physical space. This sub-structure is limited by its border Γ , which can itself be partitioned as described below.

S_d	Interface where the displacement is imposed
S_c	Interface where the stress is imposed
Γ_{pe}	Interface with an elastic medium
Γ_{pa}	Interface with an acoustic medium
Γ_{pp}	Interface with a poroelastic medium

In the case of a single porous medium, we clearly have $\Gamma_{pe} \cup \Gamma_{pa} \cup \Gamma_{pp} = \emptyset$.

12.2. Boundary problem equations

12.2.1. The $\{\mathbf{u}, \mathbf{U}\}$ formulation

We briefly recall here that the relations of the dynamics for the solid phase and the fluid phase of the homogenized porous material are given by Biot’s theory:

$$\nabla \cdot \boldsymbol{\sigma}^s = -\omega^2 (\tilde{\rho}_{11} \mathbf{u} + \tilde{\rho}_{12} \mathbf{U}), \tag{12.1a}$$

$$\nabla \cdot \boldsymbol{\sigma}^f = -\omega^2 (\tilde{\rho}_{12} \mathbf{u} + \tilde{\rho}_{22} \mathbf{U}). \quad [12.1b]$$

12.2.2. The $\{\mathbf{u}, P\}$ formulation

The $\{\mathbf{u}, P\}$ formulation was proposed by Atalla *et al.* in 1998 [ATA 98]. This formulation is based on a change of variable taking the divergence of equation [12.1b] which becomes:

$$-h\Delta P = -\omega^2 (\tilde{\rho}_{22} \nabla \cdot \mathbf{U} + \tilde{\rho}_{12} \nabla \cdot \mathbf{u}). \quad [12.2]$$

To eliminate the term with $\nabla \cdot \mathbf{U}$ Atalla *et al.* have proposed using the stress strain relation of the fluid phase. We therefore have:¹

$$\nabla \cdot \mathbf{U} = -\frac{h}{\tilde{R}} P - \frac{\tilde{Q}}{\tilde{R}} \nabla \cdot \mathbf{u}. \quad [12.3]$$

Equation [12.2] is then equivalent to the equation of motion of the fluid phase, using a $\{\mathbf{u}, P\}$ formulation,

$$\Delta P + \frac{\omega^2}{\tilde{c}^2} P - \frac{\tilde{\rho}_{22} \omega^2}{h^2} \tilde{\gamma} \nabla \cdot \mathbf{u} = 0, \quad [12.4]$$

introducing the terms,

$$\tilde{\gamma} = h \left(\frac{\tilde{\rho}_{12}}{\tilde{\rho}_{22}} - \frac{\tilde{Q}}{\tilde{R}} \right) \quad \text{and} \quad \tilde{c}^2 = \frac{\tilde{R}}{\tilde{\rho}_{22}}. \quad [12.5]$$

To eliminate the displacement of the fluid phase in the equation of motion of the solid phase, we have to eliminate the dependence on inertial terms. For this purpose, Atalla *et al.* proposed, in the harmonic system, extracting this variable from the equation of motion of the fluid phase:

$$-h\nabla P = -\omega^2 \tilde{\rho}_{22} \mathbf{U} - \omega^2 \tilde{\rho}_{12} \mathbf{u} \implies \mathbf{U} = \frac{h}{\tilde{\rho}_{22} \omega^2} \nabla P - \frac{\tilde{\rho}_{12}}{\tilde{\rho}_{22}} \mathbf{u}. \quad [12.6]$$

The second step is to eliminate the displacement variable of the fluid phase in the stress tensor of the solid phase. To do so, relationship [12.3] is used, again to define the following tensor:

$$\boldsymbol{\sigma}_{\emptyset}^s(\mathbf{u}) = \boldsymbol{\sigma}^s(\mathbf{u}, \mathbf{U}) + h \frac{\tilde{Q}}{\tilde{R}} P \mathbb{I}. \quad [12.7]$$

1. This relation can be expressed in the following way: the change in volume of the fluid phase is due to a change of pressure in the pore network, but also to the expansion of the solid phase.

We can notice that this tensor only depends on the movement of the solid phase, and is identical to the tensor of solid stresses for $P = 0$. It is also called the *in-vacuo* stress tensor. Its use permits the appearance of $\tilde{\gamma}$ in the equation of the movement of the solid phase, which yields:

$$\nabla \cdot \boldsymbol{\sigma}_0^s(\mathbf{u}) + \tilde{\rho}\omega^2\mathbf{u} + \tilde{\gamma}\nabla P = 0, \quad [12.8]$$

with the introduction of

$$\tilde{\rho} = \tilde{\rho}_{11} - \frac{\tilde{\rho}_{12}^2}{\tilde{\rho}_{22}}. \quad [12.9]$$

We now have the set of two partial differential equations (PDEs) [12.8] and [12.4] using the $\{\mathbf{u}, P\}$ formulation. We have presented the partial differential equations governing the porous materials in two formulations. We shall now see how to write the boundary conditions.

12.2.3. The boundary conditions

When writing the boundary conditions, the five types of interfaces presented above should be considered. The full description of the expressions for each formulation and each interface is not the purpose of this section. We will simply present the different values that remain unchanged and how the relationships can be found.

On the interface S_d we impose a given displacement \mathbf{u}_0 . Two relations are inferred from this condition. The first reflects the continuity of the displacement at the interface, and the second expresses the continuity of the normal displacement of the porous material and the normal displacement $\mathbf{u}_0 \cdot \mathbf{n}$. These relations are, thus, naturally written using the $\{\mathbf{u}, \mathbf{U}\}$ formulation. Since the second relation involves the movement of the fluid phase, its notation using a mixed formulation will be obtained projecting the expression [12.6] on the normal of the surface. We thus obtain:

$$\mathbf{U}|_{S_d} \cdot \mathbf{n} = \frac{h}{\tilde{\rho}_{22}\omega^2} \frac{\partial P}{\partial n} - \frac{\tilde{\rho}_{12}}{\tilde{\rho}_{22}} \mathbf{u}|_{S_d} \cdot \mathbf{n}. \quad [12.10]$$

On S_c where we impose the pressure per unit of surface P_{imp} , we use two relations on the stresses that reflect the continuity of forces on the interface as well as the continuity of the pressure. In the displacement formulation, we then have two Neumann boundary conditions on the stress tensors of the solid and fluid. In the mixed formulation, a relationship is deduced for the *in-vacuo* stress tensor and the condition of imposed pressure is naturally written.

On Γ_{pe} (interface with an elastic domain), we can write four relations. The first two equations reflect the continuity of normal stress between the two phases in contact, the third reflects the continuity of the normal displacement of the fluid phase and the last reflects the continuity of the displacement of the solid phase.

On Γ_{pa} , only three conditions are imposed. Indeed, for the acoustic environment considered consisting of a perfect fluid, which does not contribute to shear waves, there is no continuity condition of the tangential speed. The first two relationships reflect the continuity of normal stresses between the two phases in contact, the latter reflecting the continuity of the displacements, normal to the interface.

On Γ_{pp} (interface between two poroelastic phases), we can write four relations reflecting the continuity of the total stress, of the pressure, of the displacement of the solid phase and of the normal flow at the level of the interface.

These boundary problems are well posed in the cases considered in acoustics, where the porous media are open. As stated above, these equations are never directly discretized. We begin with the variational formulation of the problem.

12.3. Poroelastic variational formulations

We discuss here the several different poroelastic variational formulations. The variational formulation of the problem is equivalent to the formulation of the boundary problem based on the theorem of virtual powers. We can easily show that the boundary problem involves the variational formulation. The opposite is true only in the sense of the distributions. The advantage is that this variational formulation will be discretized in a fairly rich manner.

12.3.1. The displacement formulations

The weak integral formulation of a poroelastic domain contained in a volume Ω is given by Panneton [PAN 96a, PAN 96b]. The first step consists of multiplying each of the equations of displacement [12.1] by an admissible displacement field, i.e. verifying the corresponding boundary conditions, $\delta \mathbf{u}$ for the solid phase and $\delta \mathbf{U}$ for the fluid phase. The equations are then integrated on the volume Ω . We then obtain the two equations:

$$\int_{\Omega} \nabla \cdot \boldsymbol{\sigma}^s \delta \mathbf{u} \, d\Omega + \int_{\Omega} \omega^2 (\tilde{\rho}_{11} \mathbf{u} + \tilde{\rho}_{12} \mathbf{U}) \delta \mathbf{u} \, d\Omega = 0, \quad [12.11a]$$

$$\int_{\Omega} \nabla \cdot \boldsymbol{\sigma}^f \delta \mathbf{U} \, d\Omega + \int_{\Omega} \omega^2 (\tilde{\rho}_{12} \mathbf{u} + \tilde{\rho}_{22} \mathbf{U}) \delta \mathbf{U} \, d\Omega = 0. \quad [12.11b]$$

The first integral of each of these equations is then rewritten using Green's formula and yields:

$$\begin{aligned} & \int_{\Omega} (\boldsymbol{\sigma}^s(\mathbf{u}, \mathbf{U}) \boldsymbol{\varepsilon}^s(\delta \mathbf{u}) - \omega^2 (\tilde{\rho}_{11} \mathbf{u} \cdot \delta \mathbf{u} + \tilde{\rho}_{12} \mathbf{U} \cdot \delta \mathbf{u})) \, d\Omega \\ & = \oint_{\partial\Omega} [\boldsymbol{\sigma}^s(\mathbf{u}, \mathbf{U}) \cdot \mathbf{n}] \delta \mathbf{u} \, d\Gamma \quad \forall \delta \mathbf{u} \end{aligned} \quad [12.12a]$$

$$\begin{aligned}
 & \int_{\Omega} (\boldsymbol{\sigma}^f(\mathbf{u}, \mathbf{U}) \boldsymbol{\varepsilon}^f(\delta \mathbf{U}) - \omega^2 (\widetilde{\rho}_{22} \mathbf{U} \cdot \delta \mathbf{U} + \widetilde{\rho}_{12} \mathbf{u} \cdot \delta \mathbf{U})) d\Omega \\
 & = \oint_{\partial \Omega} [\boldsymbol{\sigma}^f(\mathbf{u}, \mathbf{U}) \cdot \mathbf{n}] \delta \mathbf{U} d\Gamma \quad \forall \delta \mathbf{U}.
 \end{aligned} \tag{12.12b}$$

This system of two equations is called the variational formulation of the poroelastic problem in motion. This construction shows clearly that the solution of the boundary problem is a solution of the variational problem.

12.3.2. Mixed formulations

In mixed formulations, the methodology to obtain the variational formulation remains the same using displacement and pressure fields. Several mixed formulations were developed and implemented. They all have, however, the same starting point which is the $\{\mathbf{u}, P\}$ formulation given by Atalla *et al.* [ATA 98]. This reads:

$$\begin{aligned}
 & \int_{\Omega} \boldsymbol{\sigma}_{\emptyset}^s(\mathbf{u}) \boldsymbol{\varepsilon}^s(\delta \mathbf{u}) d\Omega - \omega^2 \int_{\Omega} \widetilde{\rho} \mathbf{u} \cdot \delta \mathbf{u} d\Omega - \int_{\Omega} \widetilde{\gamma} \nabla P \cdot \delta \mathbf{u} d\Omega \\
 & - \oint_{\partial \Omega} [\boldsymbol{\sigma}_{\emptyset}^s(\mathbf{u}) \cdot \mathbf{n}] \delta \mathbf{u} d\Gamma \quad \forall \delta \mathbf{u},
 \end{aligned} \tag{12.13a}$$

$$\begin{aligned}
 & \int_{\Omega} \left[\frac{h^2}{\omega^2 \widetilde{\rho}_{22}} \nabla P \cdot \nabla \delta P - \frac{h^2}{\widetilde{R}} P \delta P \right] d\Omega - \int_{\Omega} \widetilde{\gamma} \mathbf{u} \cdot \nabla \delta P d\Omega \\
 & + \oint_{\partial \Omega} \left[\widetilde{\gamma} \mathbf{u} \cdot \mathbf{n} - \frac{h^2}{\widetilde{\rho}_{22} \omega^2} \frac{\partial P}{\partial n} \right] \delta P d\Gamma \quad \forall \delta P.
 \end{aligned} \tag{12.13b}$$

This original formulation was then written under several variants, that differ from each other by rewriting the boundary integrals using the divergence theorem. In 2001, Atalla *et al.* proposed an alternate layout for this formulation:

$$\begin{aligned}
 & \int_{\Omega} \left(\boldsymbol{\sigma}_{\emptyset}^s(\mathbf{u}) \boldsymbol{\varepsilon}^s(\delta \mathbf{u}) - \omega^2 \widetilde{\rho} \mathbf{u} \cdot \delta \mathbf{u} - \frac{h}{\widetilde{\alpha}} \nabla P \cdot \delta \mathbf{u} h \left(1 + \frac{\widetilde{Q}}{\widetilde{R}} \right) P \nabla \cdot \delta \mathbf{u} \right) d\Omega \\
 & - \oint_{\partial \Omega} [\boldsymbol{\sigma}^t(\mathbf{u}, P) \cdot \mathbf{n}] \delta \mathbf{u} d\Gamma \quad \forall \delta \mathbf{u},
 \end{aligned} \tag{12.14a}$$

$$\begin{aligned}
 & \int_{\Omega} \left(\frac{h^2}{\omega^2 \widetilde{\rho}_{22}} \nabla P \cdot \nabla \delta P - \frac{h^2}{\widetilde{R}} P \delta P - \frac{h}{\widetilde{\alpha}} \mathbf{u} \cdot \nabla \delta P h \left(1 + \frac{\widetilde{Q}}{\widetilde{R}} \right) \nabla \cdot \mathbf{u} \delta P \right) d\Omega \\
 & - \oint_{\partial \Omega} h (U_n - u_n) \delta P d\Gamma \quad \forall \delta P.
 \end{aligned} \tag{12.14b}$$

Without the help of the porous model, this formulation is naturally coupled with elastic or acoustic structures. It is therefore interesting to model heterogenous porous materials.

12.4. Discretized systems

The next step is to discretize the integrals involved in the variational formulations. One can express them with the nodal values of the fields and using the interpolation functions. Indeed, we have for each of the elements:

$$u^e = [N_u]^e \mathbf{u}_e \quad U^e = [N_U]^e \mathbf{U}_e, \quad [12.15]$$

where u^e and U^e are the values of the continuous field, \mathbf{u}^e and \mathbf{U}^e the values of the field at the nodes, and $[N_u]$ and $[N_U]$ correspond to form-factor functions on element e . These relationships enable us to obtain the discretization of the elementary integrals. Therefore, we can build for example:

$$\int_{\Omega} \delta \mathbf{u}^t [N_u]^e {}^t [N_u]^e \mathbf{u} d\Omega = \delta \mathbf{u}^t \left(\int_{\Omega} \delta [N_u]^e {}^t [N_u]^e d\Omega \right) \mathbf{u} = \delta \mathbf{u}^t [E_1]^e \mathbf{u}. \quad [12.16]$$

$[E_1]^e$ is called the elementary matrix. It is also possible to discretize the other integrals in the same way. Equation [12.12a] then yields:

$$\delta \mathbf{u}^t \left([\hat{\mathbf{K}}_{ss}] \mathbf{u} + [\hat{\mathbf{K}}_{sf}] \mathbf{U} - \omega^2 \tilde{\rho}_{11} [\hat{\mathbf{M}}_{ss}] \mathbf{u} - \omega^2 \tilde{\rho}_{12} [\hat{\mathbf{M}}_{sf}] \mathbf{U} - \mathbf{F}^s \right) = 0. \quad [12.17a]$$

The matrices involved in these equations were constructed by assembling elementary matrices.

$$\delta \mathbf{U}^t \left([\hat{\mathbf{K}}_{sf}]^t \mathbf{u} + [\hat{\mathbf{K}}_{ff}] \mathbf{U} - \omega^2 \tilde{\rho}_{12} [\hat{\mathbf{M}}_{sf}]^t \mathbf{u} - \omega^2 \tilde{\rho}_{22} [\hat{\mathbf{M}}_{ff}] \mathbf{U} - \mathbf{F}^f \right) = 0. \quad [12.17b]$$

The matrix of the linear problem to be solved is therefore written as:

$$\begin{bmatrix} [\hat{\mathbf{K}}_{ss}] & [\hat{\mathbf{K}}_{sf}] \\ [\hat{\mathbf{K}}_{sf}]^t & [\hat{\mathbf{K}}_{ff}] \end{bmatrix} \begin{Bmatrix} \mathbf{u} \\ \mathbf{U} \end{Bmatrix} - \omega^2 \begin{bmatrix} \tilde{\rho}_{11} [\hat{\mathbf{M}}_{ss}] & \tilde{\rho}_{12} [\hat{\mathbf{M}}_{sf}] \\ \tilde{\rho}_{12} [\hat{\mathbf{M}}_{sf}]^t & \tilde{\rho}_{22} [\hat{\mathbf{M}}_{ff}] \end{bmatrix}. \quad [12.18]$$

The poroelastic problem using the $\{\mathbf{u}, P\}$ formulation is therefore given by [ATA 98] and uses the matrix:

$$\begin{bmatrix} (1 + j\eta_s) [\mathbf{K}_{\text{int}}] + (j\omega)^2 \tilde{\rho} [\mathbf{M}_{\text{int}}] & -\tilde{\gamma} [\mathbf{C}_{\text{int}}] \\ -\omega^2 \tilde{\gamma} [\mathbf{C}_{\text{int}}]^t & \frac{h^2}{\tilde{\rho}_{22}} [\mathbf{H}_{\text{int}}] - \omega^2 \frac{h^2}{\tilde{R}} [\mathbf{Q}_{\text{int}}] \end{bmatrix}. \quad [12.19]$$

$[\mathbf{K}_{\text{int}}]$, $[\mathbf{M}_{\text{int}}]$ are associated with the stiffness matrix, and with the mass matrix of the solid phase, respectively. $[\mathbf{H}_{\text{int}}]$ and $[\mathbf{Q}_{\text{int}}]$ are associated with the matrices of kinetic energy and of compression of the fluid phase, respectively. These matrices come from discretization using the finite element method.

It is possible to make the system symmetrical², writing it as:

$$\begin{bmatrix} (j\omega)^2[\tilde{\mathbf{K}}] + (j\omega)^4[\tilde{\mathbf{M}}] & -(j\omega)^2[\tilde{\mathbf{C}}] \\ -(j\omega)^2[\tilde{\mathbf{C}}]^t & [\tilde{\mathbf{H}}] - (j\omega)^2[\tilde{\mathbf{Q}}] \end{bmatrix} \begin{Bmatrix} \mathbf{u} \\ \mathbf{P} \end{Bmatrix} = \begin{Bmatrix} \mathbf{F}^s \\ \mathbf{F}^f \end{Bmatrix}. \quad [12.20]$$

This formulation requires the construction of five global matrices. However, the obtained systems are generally ill-conditioned, due to the non-homogenous nature of the variables. Therefore, algorithms of resolution should reflect this feature. Note, however, that this does not present a limitation in modern practice because such conditions are usually able to be accepted.

12.4.1. Discussion about discretization

The resolution of a vibroacoustic problem involving an elastic structure, a fluid medium and a poroelastic medium will require discretization of each of these domains. For several reasons, the domain that will determine the size of the system is the poroelastic domain:

- Wavelengths of the Biot's waves are generally smaller than those of acoustic waves. To meet the mesh criterion of six nodes per wavelength, we will require a larger nodal density in the porous domain than in the fluid domain [DAU 01].
- The poroelastic area is meshed by volume elements, requiring a discretization in the 3 spatial directions, unlike the elements of structures – plates or shells – requiring only a mesh in 2 directions.
- The number of degrees of freedom per node of the poroelastic elements is 4 to 6 depending on whether it uses a mixed or displacement formulation, 4 to 6 times higher than a component of the fluid.

Thus, it appears that the presence of the porous material will impose some rules for the determination of an adequate mesh, these rules are quite strong for the discretization. This therefore limits the scope of such methods because it requires relatively important calculation means. Nevertheless, they are now the only way to study this type of problem [PAN 96b, DAU 03].

The comparison between the displacement formulation and the pressure formulation indicates that the number of unknowns per node is more limited for the

2. Real symmetry.

mixed formulations for an equivalent mesh. The equivalence between the required meshes to ensure the convergence of each of the formulations is a point that still needs to be studied [DAZ 08]. It is important to note that although the mixed formulation has fewer nodes, it requires the calculation of an additional matrix to take into account the volume coupling between the two phases. The construction time of the systems to be resolved is therefore more important. However, for large scale problems the most expensive step, in terms of computation time, is the resolution of the linear system that is directly linked to the number of degrees of freedom of the system. The mixed formulations therefore seem more interesting in terms of computation time, but they are more difficult to address – especially for a programmer unfamiliar with this domain. In regards to the discretization, the usual linear elements provide satisfactory results for a fluid, but may not correctly converge for a poroelastic material. These elements do not correctly take into account the shear and bending deformations. To correct this defect, the order of the functions of interpolation can be increased using quadratic elements, or hierarchical finite elements. These elements can converge without refining the mesh. However, the elementary matrices require a greater calculation time – depending on the order of these matrices. Another method consists of using modified linear elements so that deformations shearing and bending are properly taken into account. Due to the size of systems to be solved, the use of finite poroelastic elements remained until recently limited to reduce-sized configurations that can give a good representation of real structures. This drives to the development and the use of simplified models [DAU 03, DOU 07, DAZ 09]. Nevertheless, the arrival of powerful means of calculation at affordable prices now permits us to relatively easily address the complex problems stated in the introduction. Note that recently, a new displacement formulation proposed by Dazel [DAZ 07] allows the use of a much more efficient resolution method based on normal modes [DAZ 09].

12.5. Conclusion

This section was designed to introduce the numerical modeling of porous materials, using the finite element method. After presenting the historical context, the relevant problems with the boundary conditions have been recalled, then poroelastic variational formulations have been presented. The discretization of these variational formulations was then exposed and discussed. Possible examples of such techniques will be presented in Chapter 28.

12.6. Bibliography

- [ATA 98] ATALLA N., PANNETON R. and DEBERGUE P., “A mixed displacement-pressure formulation for poroelastic materials”, *J. Acoust. Soc. Am.*, vol. 104, no. 3, pp. 1444–1452, 1998.
- [DAU 01] DAUCHEZ N., SAHRAOUI S. and ATALLA N., “Convergence of poroelastic finite element based on Biot displacement formulation”, *J. Acoust. Soc. Am.*, vol. 109, no. 1, pp. 33–40, 2001.

- [DAU 03] DAUCHEZ N., SAHRAOUI S. and ATALLA N., “Investigation and modelling of damping in a plate with a bonded porous layer”, *J. Sound Vib.*, vol. 265, no. 2, pp. 437–449, 2003.
- [DAZ 07] DAZEL O., BROUARD B., DEPOLLIÉ C. and GRIFFITHS S., “An alternative biot’s displacement formulation for porous materials”, *Journ. Acoustical Society of America*, vol. 121, pp. 3509–3516, 2007.
- [DAZ 08] DAZEL O., SGARD F., BECOT F.-X. and ATALLA N., “Expressions of dissipated powers and stored energies in poroelastic media modeled by $\{u, U\}$ and $\{u, P\}$ formulations”, *J. Acoust. Soc. Am.*, vol. 123, no. 4, pp. 2054–2063, 2008.
- [DAZ 09] DAZEL O., BROUARD B., DAUCHEZ N. and GESLAIN A., “Enhanced Biot’s finite element displacement formulation for porous materials and original resolution methods based on normal modes”, accepted in *Acta Acustica-Acustica*, 2009.
- [DOU 07] DOUTRES O., DAUCHEZ N., GENEVAUX J.-M. and DAZEL O., “Validity of the limp model for porous materials: A criterion based on the Biot theory”, *J. Acoust. Soc. Am.*, vol. 122, no. 4, pp. 1845–2476, 2007.
- [COY 94] COYETTE J. and PELERIN Y., “A generalized procedure for modeling multi-layer insulation systems”, *Proceedings of the 19th International Seminar on Modal Analysis*, pp. 1189–1199, 1994.
- [COY 95] COYETTE J. and WYNENDAELE H., “A finite element model for predicting the acoustic transmission characteristics of layered structures”, *Proceedings of Inter-Noise 95*, pp. 1279–1282, 1995.
- [HÖR 03] HÖRLIN N.-E. and GÖRANSSON P., “Complex fluid displacement behaviour of a layered porous material”, *Tenth International Congress on Sound and Vibration*, Stockholm, Sweden, pp. 2179–2186, 2003.
- [JOH 95] JOHANSEN T., ALLARD J.-F. and BROUARD B., “Finite element method for predicting the acoustical properties of porous samples”, *Acta Acustica*, vol. 3, pp. 487–491, 1995.
- [KAN 95] KANG Y. and BOLTON J., “Finite element modeling of isotropic porous materials coupled with acoustical finite elements”, *J. Acoust. Soc. Am.*, vol. 98, no. 1, pp. 635–643, 1995.
- [KAN 96] KANG Y. and BOLTON J., “A finite element model for sound transmission through foam-lined double-panel structures”, *J. Acoust. Soc. Am.*, vol. 99, no. 5, pp. 2755–2765, 1996.
- [KAN 97] KANG Y. and BOLTON J., “Sound transmission, through elastic porous wedges and foam layers having spatially graded properties”, *J. Acoust. Soc. Am.*, vol. 102, no. 6, pp. 3319–3332, 1997.
- [KAN 99] KANG Y., GARDNER B. and BOLTON J., “An axisymmetric poroelastic finite element formulation”, *J. Acoust. Soc. Am.*, vol. 106, no. 2, pp. 565–574, 1999.
- [PAN 96a] PANNETON R., Modélisation numérique tridimensionnelle par éléments finis des milieux poroélastiques, PhD Thesis, University of Sherbrooke, Canada, 1996.

- [PAN 96b] PANNETON R. and ATALLA N., “Numerical prediction of sound transmission through multilayer systems with isotropic poroelastic materials”, *J. Acoust. Soc. Am.*, vol. 100, no. 1, pp. 346–354, 1996.
- [PAN 97] PANNETON R. and ATALLA N., “An efficient finite element scheme for solving the three-dimensional poroelasticity problem in acoustics”, *J. Acoust. Soc. Am.*, vol. 101, no. 5, pp. 3287–3298, 1997.
- [RAV 98] RAVIART P.-A. and THOMAS J.-M., *Introduction À L’analyse Numérique Des Équations Aux Dérivées Partielles*, Dunod, 1998.
- [SGA 02] SGARD F., *Modélisation Par Éléments-Finis Des Structures Multi-Couches Complexes Dans Le Domaine Des Basses Fréquences*, PhD Thesis, Claude Bernard University Lyon I – INSA Lyon, 2002.
- [VIG 97] VIGRAN T., KELDERS L., LAURIKS W., LECLAIRE P. and JOHANSEN T., “Prediction and measurements of the influence of boundary conditions in a standing wave tube”, *Acta Acustica*, vol. 83, pp. 419–423, 1997.
- [ZIE 89] ZIENKIEWICZ O.-C. and TAYLOR R.-L., *The Finite Element Method: Basic Formulation and Linear Problems*, 4th edition, vol. 1, McGraw-Hill, London, Great Britain, 1989.

Chapter 13

Transducer for Bulk Waves

13.1. Introduction

The experimental study of acoustic wave propagation requires devices called transducers, which are able to generate these waves and detect them efficiently. The means used depend on the practical constraints and technological possibilities. For example, if no mechanical contact with the sample is allowed, a solution is to generate bulk or surface acoustic waves with a laser pulse and to detect it after propagation by optical interferometry [ROY 96a]. At low frequencies ($f < 1$ MHz) and when the acoustic impedance Z of the propagation medium is relatively small ($Z < 10$ MRayl.), the coupling with the transducer can be achieved thanks to the air [SCH 95].

In most cases, the transducer is a damped electromechanical resonator consisting of a piezoelectric solid carrying two electrodes, either in direct contact with the propagation medium, or through a liquid (water). A plate of large lateral dimensions compared to the wavelength λ and of thickness d of the same order of magnitude as $\lambda/2$ generates plane bulk waves, preferentially at the frequency $f_P = V_P/2d$ where V_P is the speed of the elastic waves (longitudinal or transverse) in the piezoelectric material. The operation of such a transducer can be analyzed according to a one-dimensional model [KIN 87]. Before developing this model, we note the essential properties of the propagation of elastic waves in a piezoelectric medium. Examples of impulse and frequency responses are given in the last section.

13.1.1. Piezoelectric materials – structures

The piezoelectric material is the key element of a transducer because it converts electrical energy from an external source into acoustic energy which can be used in the form of a bulk wave propagating in the medium that we consider and vice versa.

Piezoelectricity reflects the linear dependence between the mechanical and electrical properties of some anisotropic materials. The direct piezoelectric effect, discovered by Pierre and Jacques Curie in 1880, expresses the appearance of a polarization, i.e. an electrical induction D , in a dielectric subjected to a strain S :

$$D = \epsilon^S E + eS. \quad [13.1]$$

ϵ^S and e are, respectively, the dielectric constant (at a constant strain) and the piezoelectric constant. The inverse piezoelectric effect, predicted by Lippman one year later, indicates that a piezoelectric solid placed in an electrical field distorts itself. The mechanical stress T is expressed by the formula:

$$T = c^E S - eE, \quad [13.2]$$

which generalizes Hooke's law (equation [1.43]). c^E is the stiffness constant when the electrical field is held constant. The fact that the proportionality coefficients for the two effects are opposite to each other [ROY 96b] results from thermodynamic considerations. The first effect is used to detect elastic waves, the second one for generating them.

With tensor notation and using the summation convention on the repeated indices, the behavior laws of a piezoelectric solid are written:

$$T_{ij} = c_{ijkl}^E S_{kl} - e_{kij} E_k \quad \text{and} \quad D_j = \epsilon_{jk}^S E_k + e_{jkl} S_{kl}. \quad [13.3]$$

Due to the symmetry of the strain tensor ($S_{kl} = S_{lk}$), the piezoelectric tensor, of rank 3, has only 18 components $e_{j\alpha}$ with $j = 1$ to 3 and $\alpha = 1$ to 6. The index α corresponds to the pair (kl) according to the following correspondence:

$$(11) \rightarrow 1, (22) \rightarrow 2, (33) \rightarrow 3, (23) = (32) \rightarrow 4, (13) = (31) \rightarrow 5, (12) = (21) \rightarrow 6.$$

These constants can be set out in a 3×6 table and their values are typically between 0.1 and 20 C/m².

$$e_{i\alpha} = \begin{vmatrix} e_{11} & e_{12} & e_{13} & e_{14} & e_{15} & e_{16} \\ e_{21} & e_{22} & e_{23} & e_{24} & e_{25} & e_{26} \\ e_{31} & e_{32} & e_{33} & e_{34} & e_{35} & e_{36} \end{vmatrix} \quad [13.4]$$

The ability of a piezoelectric material to generate elastic waves is measured by its electromechanical coupling coefficient K . This coefficient expresses the influence of the piezoelectricity on the velocity V of the elastic waves, by definition:

$$K^2 = \frac{V^2 - V'^2}{V^2} \quad [13.5]$$

where V' is the velocity calculated without taking account the piezoelectric effect.

The equations of propagation result from the application of Newton's second law and Poisson's equation, which governs quasi-static electrical phenomena:

$$\frac{\partial T_{ij}}{\partial x_j} = \rho \frac{\partial^2 u_i}{\partial t^2} \quad \text{and} \quad \frac{\partial D_j}{\partial x_j} = \rho_e, \quad [13.6 \text{ and } 13.7]$$

where ρ is the mass density and ρ_e the density of free charges.

Given the expressions of the strain S_{ij} and of the electric field E_k as functions of the mechanical displacement u_l and the electrical potential ϕ :

$$S_{kl} = \frac{1}{2} \left(\frac{\partial u_l}{\partial x_k} + \frac{\partial u_k}{\partial x_l} \right) \quad \text{and} \quad E_k = -\frac{\partial \phi}{\partial x_k}, \quad [13.8]$$

and substituting in equations [13.3] leads, in the absence of electrical sources ($\rho_e = 0$), to four homogeneous second-order differential equations ($i = 1, 2, 3$):

$$\begin{cases} \frac{\partial^2}{\partial x_j \partial x_k} (c_{ijkl} u_l + e_{kij} \phi) = \rho \frac{\partial^2 u_i}{\partial t^2} \\ \frac{\partial^2}{\partial x_j \partial x_k} (\varepsilon_{jkl}^S \phi - e_{jkl} u_l) = 0. \end{cases} \quad [13.9]$$

The solution in the form of plane waves, with a polarization p_l , propagating in the direction of the unit vector n_j at the phase velocity $V = \omega/k$:

$$u_i = p_i \exp i(\omega t - kn_j x_j) \quad \text{and} \quad \phi = \phi_0 \exp i(\omega t - kn_j x_j) \quad [13.10]$$

leads, by writing

$$\Gamma_{il} = c_{ijkl}^E n_j n_k, \quad \gamma_l = e_{jkl} n_j n_k, \quad \varepsilon^S = \varepsilon_{jk}^S n_j n_k, \quad [13.11]$$

to the system of equations ($i = 1, 2, 3$)

$$\Gamma_{il} p_l + \gamma_i \phi_0 = \rho V^2 p_i \quad \text{and} \quad \gamma_l p_l - \varepsilon^S \phi_0 = 0, \quad [13.12]$$

which generalizes the Christoffel equations (section 1.2.2) that describe the behavior of a non-piezoelectric material. The elimination of the electric potential ϕ_0 leads to

$$\bar{\Gamma}_{il} p_l = \rho V^2 p_i \quad \text{with} \quad \bar{\Gamma}_{il} = \Gamma_{il} + \frac{\gamma_i \gamma_l}{\varepsilon^S}. \quad [13.13]$$

The velocity V and the polarization p_l of the plane elastic waves propagating in a piezoelectric solid can be obtained by looking for the eigenvalues and eigenvectors of the Christoffel matrix $\bar{\Gamma}_{il}$. Since this matrix is symmetric, the three eigenvalues are real and the eigenvectors are mutually orthogonal. The velocity of the three plane waves propagating in the same direction are solutions of the secular equation:

$$\det[\bar{\Gamma}_{il} - \rho V^2 \delta_{il}] = 0. \quad [13.14]$$

In an anisotropic medium, the propagation of plane elastic waves is illustrated by the slowness surface, obtained from the vector $\mathbf{m} = \mathbf{n}/V$ drawn from an arbitrary origin O . It is composed of three layers, one for the quasi-longitudinal wave and one for each transverse or quasi-transverse wave (section 1.2.2.3).

Figure 13.1 refers to lithium niobate (LiNbO_3) which belongs to the trigonal class $3m$. The dashed curves have been calculated ignoring the piezoelectric effect. The transverse wave (T) polarized along the X -axis, perpendicular to the propagation plane YZ , is not piezoelectrically coupled ($V = V'$). For the other two modes (QL and QT), the difference between the solid and dashed curves, illustrates the electromechanical coupling.

By multiplying the Christoffel equation [13.12] by the complex conjugate p_i^* of the polarization, which is assumed to be normalized ($p_i p_i^* = 1$), it becomes:

$$\rho V^2 = \Gamma_{il} p_l p_i^* + \frac{|\gamma_i p_i|^2}{\epsilon^S} \quad \text{and} \quad \rho V'^2 = \Gamma_{il} p_l' p_i'^* . \quad [13.15]$$

As the polarizations p_i and p_i' are similar (they are identical if the mode is purely longitudinal or transverse), the square of the electromechanical coupling coefficient [13.5] can be written as

$$K^2 = \frac{|\gamma_i p_i|^2}{\epsilon^S \Gamma_{il} p_l p_i^* + |\gamma_i p_i|^2} = \frac{e^2}{\epsilon^S c^E + e^2} \quad [13.16]$$

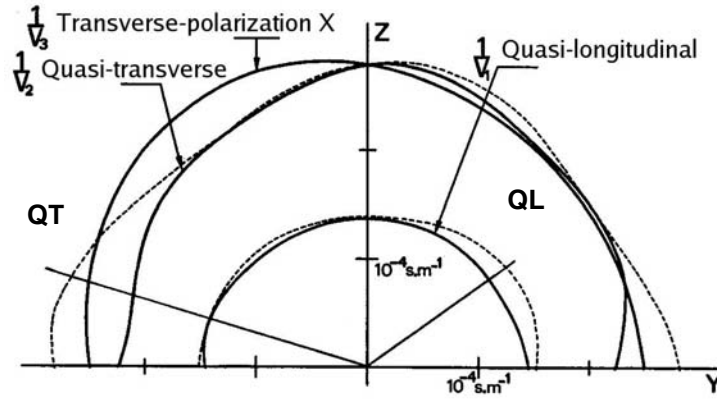


Figure 13.1. Section of the slowness surface of lithium niobate in the YZ plane. The dashed curves do not take into account the piezoelectric effect.

where $e = |\gamma_i p_i|$ has the dimension of a piezoelectric constant and $c^E = \Gamma_{il} p_l p_i^*$ of a stiffness constant. This coefficient (less than unity) is also expressed as a function of the average densities of the acoustic and electrical potential energies:

$$\begin{cases} e_p^{(ac)} = \frac{1}{2} c_{ijkl} S_{ij} S_{kl}^* = \frac{1}{2} \Gamma_{il} p_i^* p_l k^2 \\ e_p^{(el)} = \frac{1}{2} \epsilon_{jk}^S E_j E_k^* = \frac{1}{2} \epsilon^S |\phi_0|^2 k^2 = \frac{1}{2\epsilon^S} |\gamma_i p_i|^2 k^2 . \end{cases}$$

From [13.16]

$$K^2 = \frac{e_p^{(el)}}{e_p^{(ac)} + e_p^{(el)}}$$

the square of the electromechanical coupling coefficient is the ratio of the electric potential energy to the total potential energy. This factor characterizes the ability of the piezoelectric material to generate acoustic waves. Indeed, whatever its polarization, the electric field associated with a plane wave is longitudinal. The inverse piezoelectric effect, plane acoustic waves are generated by applying an electric field perpendicular to the face of the plate. For example, the curves in Figure 13.1 show that a quasi-longitudinal (QL) wave is generated selectively by a crystal plate having a cut $Y + 36^\circ$ ($K_L = 0.49$, $K_T = 0$) and a quasi-transverse (QT) wave is generated selectively by a plate of cut $Y + 163^\circ$ with a coupling coefficient $K_T = 0.62$ ($K_L = 0$).

The *structure* of the transducer (Figure 13.2) and the choice of the piezoelectric material, whose thickness is a fraction of the wavelength λ , depend on the frequency of the waves to be generated and of the propagation medium (solid or liquid). It is characterized by its acoustic impedance $Z = \rho V$, which is expressed in MRayl. (10^6 Rayl.).

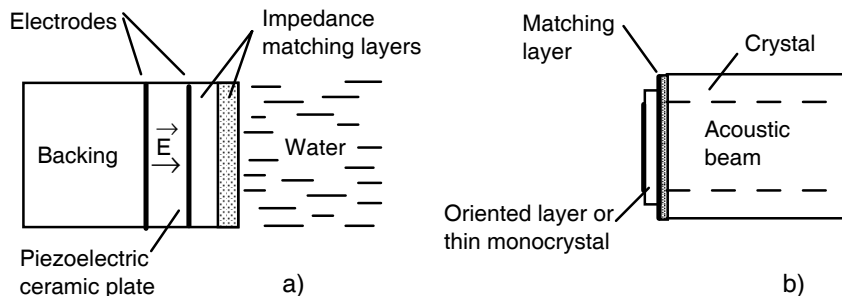


Figure 13.2. Structure of a single element plane transducer used to generate bulk waves, a) at low frequencies ($f < 25$ MHz), b) at intermediate and high frequencies ($f > 25$ MHz)

Low frequencies ($f < 25$ MHz $\rightarrow \lambda/2 > 0.1$ mm). The material is very often a piezoelectric ceramic plate whose faces are metal-coated and loaded on the back with an absorbing medium that damps the resonator and consequently widens the bandwidth (Figure 13.2a). However, in non-destructive testing and in medical ultrasound, the acoustic impedance of piezoelectric ceramics ($Z_P \geq 30$ MRayl. with $V_P \cong 4,500$ m/s and $\rho_P \cong 7,500$ kg/m³) is too large compared to that of the propagation medium (water or the human body: $Z \cong 1.5$ MRayl. with $V \cong 1,500$ m/s

and $\rho \cong 10^3 \text{ kg/m}^3$). The mechanical matching between the transducer and the propagation medium, which is needed to increase the efficiency of the “electrical energy \leftrightarrow mechanical energy” conversion, requires the use of intermediate layers. One way to reduce the number of matching layers is to use a *piezocomposite material*. The transducer is composed of active ceramic elements, in the form of rods, for example, embedded in a passive resin, with a much smaller acoustic impedance (3 MRayl.). The overall impedance of the transducer is thereby lower (5 to 15 MRayl., for a volume fraction of ceramic between 15 and 50%). Contrary to appearance, the electromechanical coupling coefficient is larger than that of a homogeneous plate. Indeed, for the same supply voltage, a rod surrounded by a relatively soft material vibrates more than a rod embedded in a ceramic block. Nevertheless, the piezocomposite transducer, very commonly used, has the disadvantage of a limited operating frequency ($f \leq 15 \text{ MHz}$); this results from the fact that the period of the rods in the polymer matrix must be small compared to the overall thickness. Another variety of transducers based on polymers and copolymers such as P(VDF-TrFE), a compound of vinylidene fluoride (VDF) and trifluoroethylene (TrFE), able to operate at frequencies larger than 100 MHz, present some advantages: their flexibility allows a wide range of shapes, their low acoustic impedance avoids the use of a matching layer, their low cost and availability leads to applications in medical acoustic and non-destructive testing (acoustic microscopy).

Intermediate frequencies ($25 \text{ MHz} < f < 500 \text{ MHz} \rightarrow 5 \mu\text{m} < \lambda/2 < 100 \mu\text{m}$). One technique is to paste with a resin or to solder, using indium metallic diffusion under pressure, a thick monocrystal ($>100 \mu\text{m}$), and then to reduce it to the desired thickness by polishing. Figure 13.2b shows a transducer for acoustic microscopy, acousto-optic interaction or a high frequency delay line. Due to its high electromechanical coupling coefficient, lithium niobate is often used for this kind of application.

High frequencies ($f > 1 \text{ GHz} \rightarrow \lambda/2 < 3 \mu\text{m}$). The piezoelectric material is deposited in the form of a thin layer onto the substrate already coated with a metallic film constituting the internal electrode. Most often it is a layer of zinc oxide (ZnO) or of aluminum nitride (AlN) deposited by sputtering on an alumina monocrystal (sapphire). This propagation medium undergoes very small losses at high frequencies. As the A_6 axis of ZnO is always perpendicular to the surface, the piezoelectric layer generates only longitudinal waves. In order to create high frequency transverse waves, a plate of lithium niobate of cut $Y + 163^\circ$ must be soldered by diffusion and reduced to the desired thickness (some μm) first by polishing, and then by chemical etching or ion bombardment. In this kind of transducer, the role of the electrodes, at least that of the internal electrode, must be considered.

The main piezoelectric materials and their most relevant characteristics as transducers are given in Table 13.1.

Material	Section	Polar.	V (m/s)	Z(Mrayl.)	K	ϵ^s/ϵ_0
LiNbO ₃	Y + 36°	Quasi-L	7340	34.5	0.49	38.8
LiNbO ₃	Y + 163°	Quasi-T	4560	21.4	0.62	42.8
PZT4 Ceramic	Z	L	4560	34.2	0.51	633
PZT4 Ceramic	Z	T ⊥ Z	2600	19.5	0.71	735
P(VDF-TrFE)	Z	L	2400	4.5	0.30	6.0
ZnO	Z	L	6400	36.3	0.28	8.8
AlN	Z	L	10400	34	0.17	8.5

Table 13.1. Velocity (V), acoustic impedance (Z), electromechanical coupling coefficient (K) and relative permittivity (ϵ^s/ϵ_0) for the main piezoelectric materials used as transducers

13.1.2. One-dimensional model – equivalent circuits

We assume that the thickness d of the piezoelectric slab, large compared to one of its electrodes, is small compared to its lateral dimensions. The voltage is applied (or gathered if the transducer is working in the receiving mode) between those electrodes. Under these circumstances, a one-dimensional model (without subscript of coordinates) is enough (Figure 13.3). An analysis method consists of associating this structure with an electromechanical circuit obtained by juxtaposing the equivalent circuit to the different parts, force and particle velocity playing similar roles to the voltage and the electrical intensity.

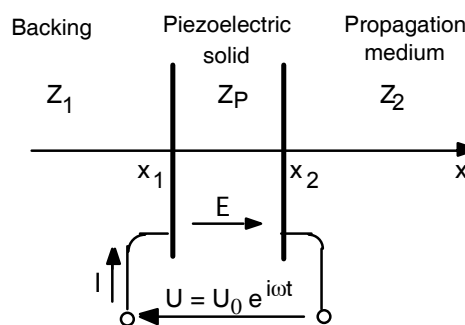


Figure 13.3. One-dimensional model of a low frequency transducer. It is divided into three parts: the propagation medium of impedance Z_2 , the piezoelectric material of impedance Z_p and the backing medium of impedance Z_1

13.1.2.1. Impedance matrix

If the conditions for the generation of a pure longitudinal or transverse wave are fulfilled, the state equations of the piezoelectric solid reduce to [13.1] and [13.2], where c^E , ϵ^S and e are appropriate constants given the orientation of the crystallographic axis and the type of wave. For example, in the case of a Z-cut piezoelectric ceramic or zinc oxide layer and for a longitudinal wave: $c^E = c_{33}^E$, $e = e_{33}$ and $\epsilon^S = \epsilon_{33}^S$.

From Poisson's equation [13.7], the electrical induction D is uniform in the insulating piezoelectric solid ($\rho_e = 0 \rightarrow \partial D / \partial x = 0$). The charge conservation equation imposes a uniform current density j :

$$\frac{\partial D}{\partial t} = j(t) = \frac{I(t)}{A},$$

where I is the current intensity and A the area of the electrodes.

Eliminating the electric field E in equations [13.1] and [13.2] in order to express the stress as a function of the electrical induction D

$$T = c^D \frac{\partial u}{\partial x} - hD, \quad \text{where} \quad h = \frac{e}{\epsilon^S} \quad [13.17]$$

and introducing the stiffness at constant electrical induction $c^D = c^E + e^2/\epsilon^S$. By differentiating with respect to time, we obtain the particle velocity $v = \partial u / \partial t$:

$$\frac{\partial T}{\partial t} = c^D \frac{\partial v}{\partial x} - \frac{h}{A} I(t). \quad [13.18]$$

Differentiating equation [13.17] with respect to x and considering dynamic equation [13.6], leads to:

$$c^D \frac{\partial^2 v}{\partial x^2} = \rho \frac{\partial^2 v}{\partial t^2}. \quad [13.19]$$

The solution of this equation of propagation is the sum of two waves, of amplitudes a and b , propagating in opposite directions at velocity $V = \sqrt{c^D / \rho}$; in the harmonic regime and omitting the factor $e^{i\omega t}$:

Chapter 31

Use of Time-reversal

31.1. Use of time-reversal

Because of its ability to learn to focus in an adaptive way in a very short time in complex heterogenous media, time-reversal can be applied successfully in the domain of imaging and ultrasound therapy [FIN 03]. It can be used to correct the distortions induced by the skull on the therapy beam in a treatment of brain tumors by focused high intensity ultrasound. It is also able to learn to follow in real-time the movements of a kidney stone during a lithotripsy treatment, and also to detect, with a better accuracy than conventional ultrasound imaging, the micro-calcifications present in the breast. Applying the principle of time-reversal, focusing on resonant cavities allows, thanks to the great impact of temporal compression of ultrasonic signals, a large increase in the amplitude of the overpressure created by conventional transducers for the destruction of kidney stones.

31.1.1. Monitoring and destruction of kidney stones by time-reversal

Extracorporeal ultrasound lithotripsy (destruction of kidney stones or renal lithiasis or gallbladder) appeared in 1980 and can now handle the bulk of renal lithiasis. Nevertheless, although lithiasis can be located precisely with X-ray imaging, existing systems are unable to track in real-time the movements of tissue caused by the breathing of the patient. It is estimated that more than 66% of the shots miss their target and cause damage to surrounding tissues such as local hemorrhage.

31.1.1.1. *Correction of respiratory movements by time-reversal*

The principle of adaptive focusing by time-reversal is particularly well suited to this problem. Indeed, the destruction of kidney stones is classically done with an ultrasound beam created by a single spherical piezoelectric dome focused permanently on the same position. However, during treatment, it appears that the patient's respiratory movements move the desired target, which very often moves out of the focus zone of the stone. It is known that less than 20% of the ultrasonic shots actually reach the kidney stone, resulting in an important loss of efficiency and in quite long treatment periods. The Laboratoire Ondes et Acoustique at ESPCI (Paris, France) has developed a time-reversal mirror to track the movements of the stone, and thereby ensure that all the ultrasonic beams effectively reach the desired target. The kidney stone is used as a passive acoustic source, on which the time-reversal mirror learns to “autofocus” (see sections 15.1.2 and 15.1.5).

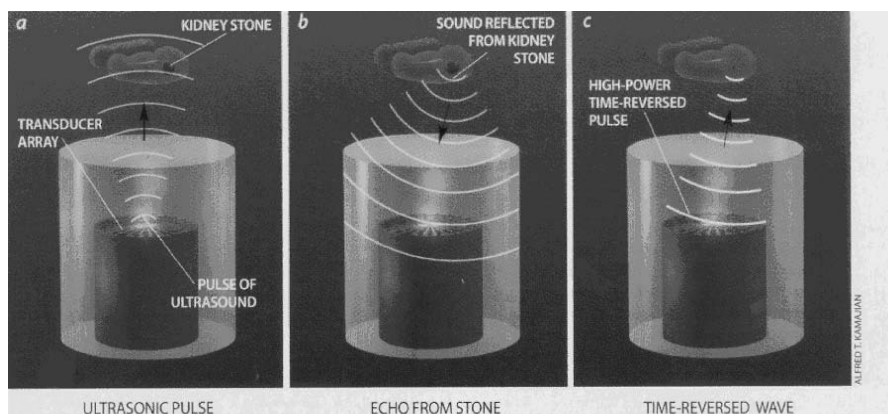


Figure 31.1. *Tracking of the movements of a kidney stone through the technique of adaptive focusing by time-reversal*

It is indeed possible, using the method presented in Figure 31.1, to force the system to focus in real time on the desired target. A first wave is emitted, by the array of piezoelectric transducers, of high-electric power (a). Then the backscattered waves mainly come from the kidney stone, because of its great reflectivity compared to the surrounding tissue (b). The backscattered signals are time-reversed and reissued by the transducer array. The ultrasound beam refocuses then naturally on the kidney stone (c). Because of the rapid propagation of ultrasound ($1500 \text{ m}\cdot\text{s}^{-1}$), this operation can be repeated over 100 times per second. As the movements caused by the breathing of the patient are much slower, it ensures that the ultrasound beam remains focused on its target.

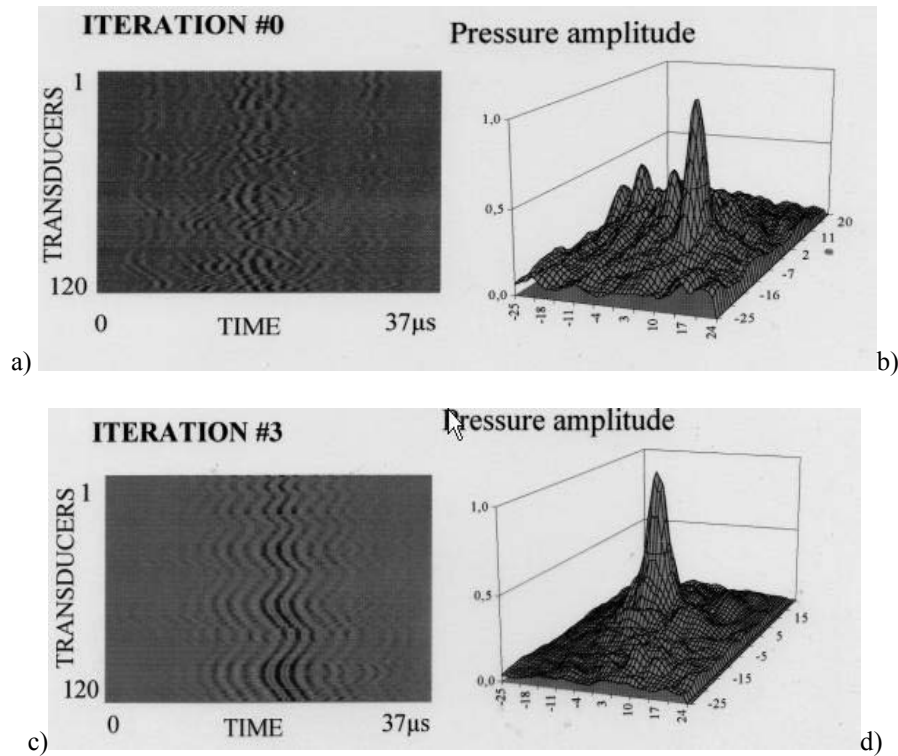


Figure 31.2. Ultrasonic echoes received on the transducer array after one (a) and three (c) iterations of the time-reversal process. Spatial distributions of the ultrasound beam in the focalization plane at the first (b) and third (d) iteration

As shown in Figure 31.2, after a few iterations of the time-reversal focalization process, the echoes from the target are perfectly selected compared to echoes from the surrounding tissue, and the quality of the focus beam slims down on the kidney stone. These iterations of the process take place in a very short time (a few tens of μs) and ensure that the ultrasound beam remains permanently focused on the target.

A first prototype including an electronic device of 64 channels operating in parallel has been made in recent years, in collaboration with the company Technomed. The numerous *in vitro* experiments on kidney stones and gallstones have proved its efficiency. The time-reversal mirror helps to locate the lithiasis in less than 40 ms, thus providing real-time monitoring.

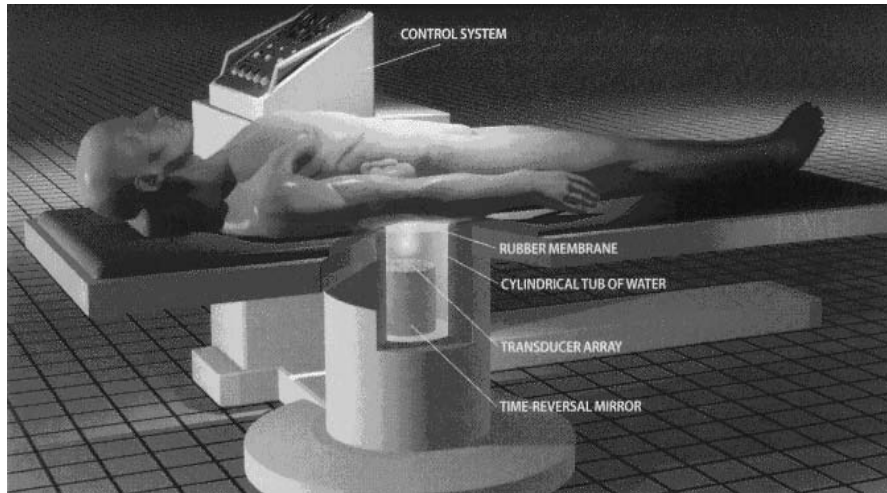


Figure 31.3. *Futuristic vision of a time-reversal mirror for the destruction of kidney stones*

Clinical trials at the Cochin hospital in Paris (for nephritic lithiasis) and the Edouard Herriot hospital in Lyon (for cholelithiasis) have also given very encouraging results. We can thus follow the movements of lithiasis in real time. Such a system in its final version could look like the illustration shown in Figure 31.3 [FIN 99].

Due to the large number of piezoelectric transducers necessary to ensure both i) an extremely important overpressure at the acoustic focus, and ii) a capacity of electronic movement of the focal point by several centimeters around the initial focal position, the price of such a system remains prohibitive so far.

31.1.1.2. *Time-reversal and ultrasonic pulse compression*

To remedy this shortcoming, time-reversal focusing may also be used to reduce very substantially the number of necessary transducers to develop such a system. This significant improvement is based on the exploitation by time-reversal processing of the many reverberations of an ultrasonic wave in a solid waveguide [MON 02]. The new system consists of a small number of piezoelectric transducers glued to one end of a solid Duralumin waveguide (see Figure 31.4). The other end of the solid tube is against the skin of the patient.

The acoustic signal coming from a source located at the desired focal point (i.e. from the kidney stone) suffers a big temporal dispersion during its propagation through the solid tube. The signal received by the transducers can have a temporal length 1,000 times larger than the initial impulse (see Figure 31.5b).

After time-reversal and re-emission by the transducers, the resulting wave focuses on the focus point, just as if we were replaying the film of wave propagation in reverse order. Thus, all the energy contained in a signal of several milliseconds is recompressed at the focus to form a signal of a few microseconds.

The result is a huge amplification of the signal, which then ensures the destruction of the stone by mechanical effect. This amplification of the focused signal by time-reversal in a reverberant medium is the acoustic analog of the amplification of light in femtosecond lasers.

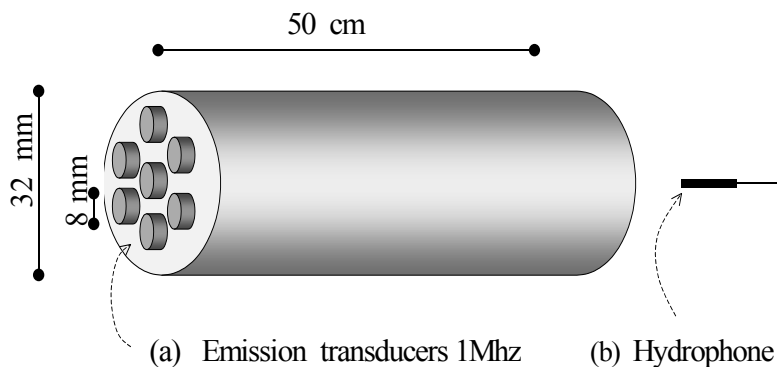


Figure 31.4. Principle of amplification of ultrasonic signal by pulse compression

Two prototypes have been developed and a maximum gain of 15 (in terms of the acoustic overpressure at the focus) has been experimentally measured. Through the use of reverberations in the solid tube, it should be possible in the future to reduce the number of necessary transducers for real-time tracking of kidney stones by a factor greater than 20!

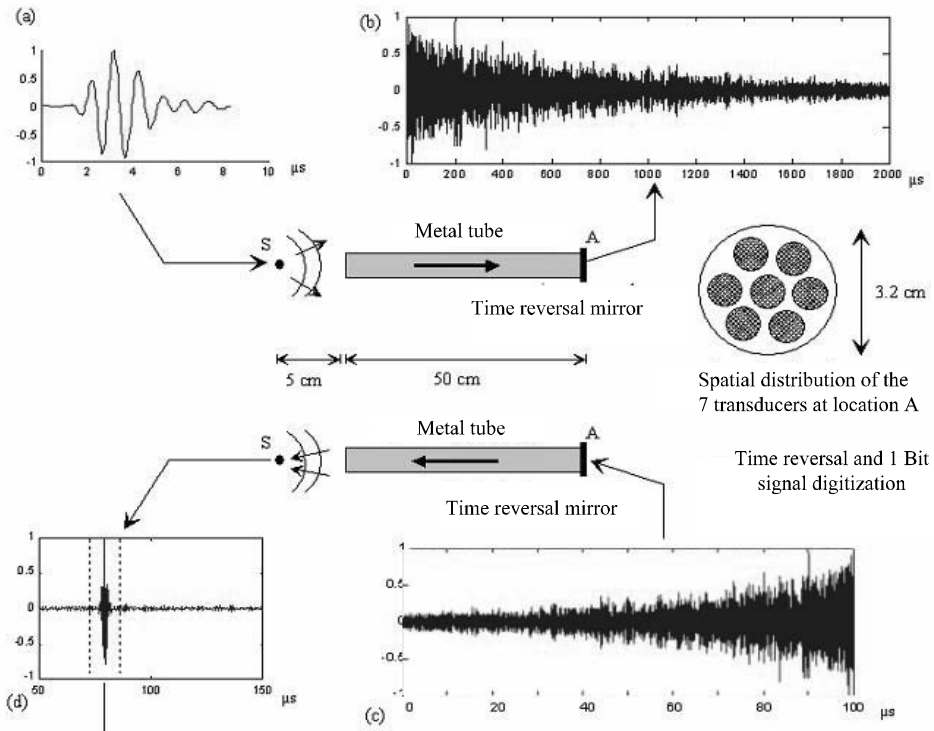


Figure 31.5. Principle of ultrasound amplification by temporal recompression. (a) During the calibration phase, seven transducers of the array record the temporal signal coming from an ultrasound source. (b) the signal is stored in memory. During the experiment, we emit a temporally-reversed signal. This refocuses all the energy of the emission signal at the focal point in a very short time. There is a great temporal compression, which greatly increases the amplitude of the signal at the focus

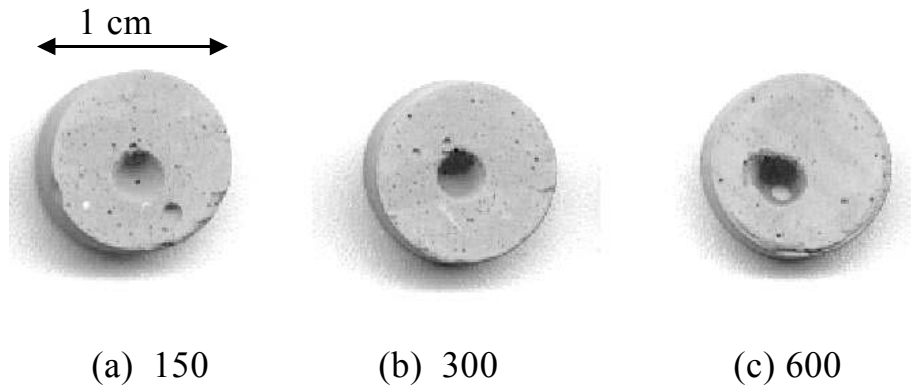


Figure 31.6. *Impacts of the ultrasound beam on a piece of chalk for 150, 300 and 600 successive insonifications*

31.1.2. *Ultrasound focalization in the brain by time-reversal*

Non-invasive brain surgery using ultrasonic beams is certainly the application for which the contribution of the principle of time-reversal focusing is the most invaluable.

Devices for extracorporeal “surgery” of cancerous brain tumors, for which conventional surgery is too delicate, are currently under development. Their mechanism is based on the use of a focused ultrasound wave to create, at the acoustic focus, a temperature rise sufficient to destroy cells. This focused ultrasound wave is generated by an array made of a large number of piezoelectric transducers spread over an area surrounding the skull [TER 01].

However, the realization of such a focused ultrasound beam is difficult, due to the heterogeneities of biological tissues crossed. In this application, the difficulties are intensified by the large discrepancy between ultrasound speeds in bone and in soft tissues, and also by the significant loss of energy when crossing the bone. This leads to a significant deterioration, or even a deviation of the beam. This constraint involves a focus that fits the medium, and therefore requires the use of an array of piezoelectric transducers operating with an electronic focus. The technique of time-reversal focusing helps to achieve excellent results in terms of correction of the emission beam in these extreme conditions [TAN 98].

Note however that the principle of time-reversal takes advantage of the time-reversal invariance of the wave equation in non-dissipative media. But apart from its heterogeneities in speed of sound and density, the skull is also a medium with absorption heterogeneities. Ultrasound absorption degrades the quality of the focusing by time-reversal. The time-reversal process can be modified to take into account this absorption phenomena in the bone of the skull; this approach may also be extended by a new technique of adaptive focusing called spatio-temporal reverse filtering, which helps to totally correct the damage caused by the bone of the skull on the focused ultrasound beams. This technique generalizes the time-reversal focusing to absorbent media.

31.1.2.1. *Adaptive focusing: time-reversal and biopsy*

The use of time-reversal mirrors is particularly suited for brain therapy. Time-reversal, however, requires the presence at the focal point of an acoustic source, a sensor or a reflector, on which the system initially learns to make an “autofocus”. This reference can be provided during the biopsy, which is a minimally intrusive surgical intervention, made before most major surgery. A tiny acoustic source would be placed at the end of the surgical instrument intended to take a sample of tissue. The treatment then consists of putting the system in adjustment on such a reference throughout the heterogenous medium by issuing a pulse signal from this small acoustic source. The signals received on the transducer array, located against the cranial wall, are stored in memory, and the tiny acoustic source, connected to the surgical instrument, is removed. These received signals are then used to calculate the temporal codes to issue to each element of the array. These emission codes are stored in memory pending the outcome of the biopsy. The system can again focus on the reference point, but the focal point can also be moved electronically around this position to explore the entire tumor. The focalizations obtained have an identical quality to those obtained in a homogeneous medium, and have been obtained up to side-lobe levels of -20 dB. This contrast is quite sufficient for therapy, where the temperature rise is proportional to the energy provided, and is therefore obtained with a contrast larger than 100. On the other hand, the focal point has been moved more than 15 mm on both sides of the reference location, keeping a very good contrast.

31.1.2.2. *Simulated time-reversal: ultrasound focalization guided by X-ray imaging*

To be completely free from the biopsy stage and work in a totally non-invasive way, we can also be guided by Scanner X-ray imaging. It is indeed possible to completely achieve the first stage of time-reversal focusing by simulation. For that, we can use codes from numerical simulation by finite differences, helping to model the propagation of ultrasonic waves in various types of complex heterogenous and absorbent media.

X-ray imaging of the skull of the patient may indeed bring us the input parameters necessary for this calculation code (speed of sound, density of bones, and ultrasonic absorption) to completely model the propagation of ultrasonic waves through the skull. Thus, conducting an examination by X-rays helps to totally model the propagation of the ultrasound beam through the skull.

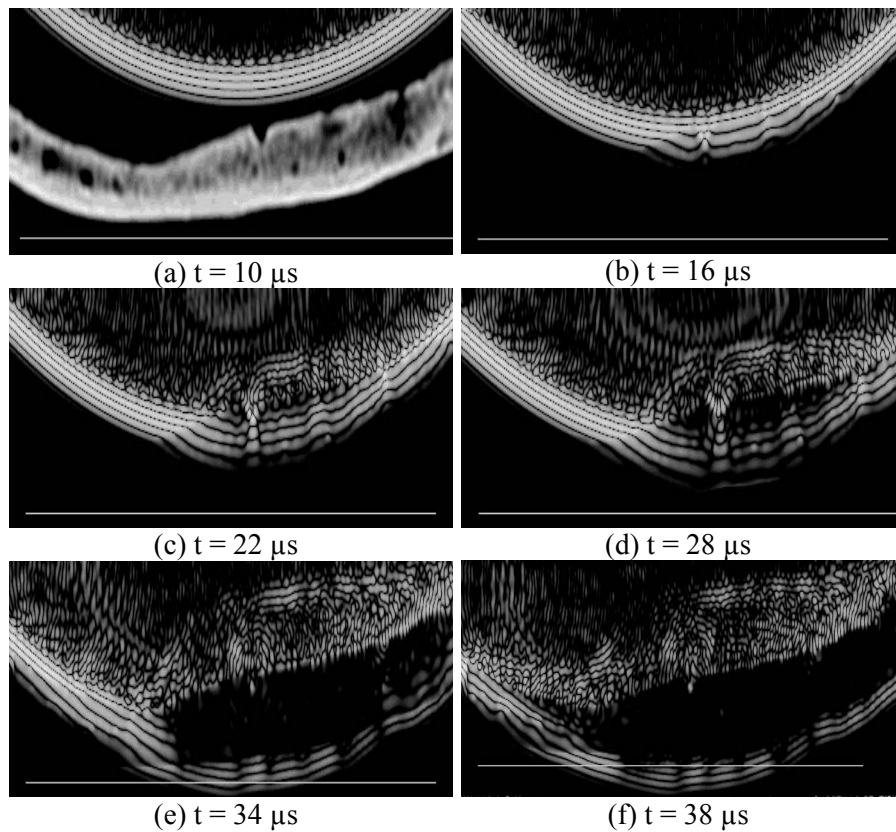


Figure 31.7. Numerical simulation of the propagation of a focused ultrasound wave through the bone structure of the skull: two-dimensional image of the ultrasound field at different moments. The acoustic parameters are deduced from the X-ray image of the skull

As shown in Figure 31.8, the correlation between numerical simulations and experiments is extremely good. It will therefore be possible in the near future to be free from the biopsy stage and to make a totally extracorporeal treatment of brain tumors.